ArduHydro: A Low-Cost Device for Water Level Measurement and Monitoring

Andrea Galli (andrea.galli@fondazionepatrimoniocagranda.it)
Fondazione Patrimonio Ca' Granda
Cosimo Peruzzi
Italian Institute for Environmental Protection and Research (ISPRA)
Fabiola Gangi
University of Milan
Daniele Masseroni
University of Milan

Research Article

Keywords: Low-cost sensor, water level, Arduino, monitoring, irrigation

Posted Date: November 21st, 2022

DOI: https://doi.org/10.21203/rs.3.rs-2252311/v1

Additional Declarations: No competing interests reported.

Version of Record: A version of this preprint was published at Journal of Agricultural Engineering on January 23rd, 2024. See the published version at https://doi.org/10.4081/jae.2024.1554.

Abstract

ArduHydro is a low-cost device for water level measurement and monitoring designed for a short and long-term employment in controlled and outdoor environments. It measures water level through an ultrasonic sensor and elaborates the signals through an Arduino micro controller. The small size of this device, the low energy required for its operation, its robustness and accuracy make ArduHydro properly versatile for different applications in the field for water control and management. This article describes the design, the components, the costs, and the performance of ArduHydro. Performance was assessed with a laboratory test inside a hydraulic circuit constituted by an open channel flume and comparing ArduHydro measurements with those obtained with a traditional ultrasonic sensor. An example of ArduHydro application for detecting the wavefront evolution during a surface irrigation is presented as well. The results revealed that ArduHydro measurements were on average very consistent with those obtained by the traditional ultrasonic sensor in all different flow conditions (i.e. different flowrate and water depth) demonstrating its reliability and accuracy in the measuring water level. The application of ArduHydro during a surface watering of an agricultural field allowed to obtain important spatio-temporal information about the water depth along the longitudinal direction of the field, paying the way for a real comprehension of the dynamics of wavefront evolution in a real-world case study.

1 Introduction

The acquisition of on-field data is a crucial task in many research areas and, over time, the necessity to gather data with higher spatial and temporal resolutions is emerging (Montanari et al., 2013). In recent years, and particularly in environmental sciences, this hunger for data has found a significant help in the so-called low-cost monitoring systems (Mao et al., 2019; Tauro et al., 2018; Toran, 2016; Tscheikner-Gratl et al., 2019; Wickert et al., 2019). Considering the definition provided by Cherqui et al. (2020), the jargon *low-cost technology* refers to systems that have a substantially lower price than traditional/commercial technology. The reasons to use low-cost monitoring systems are numerous and not only linked to affordability: for instance, these technologies are also fully customizable, open-source, and allow users not to rely on proprietary technologies developed by a specific commercial company (Fisher & Gould, 2012; Mao et al., 2019). For the abovementioned reasons, the research for novel low-cost technologies that are more versatile and cheaper in comparison to commercial equipment is a trending topic in recent years (Fisher et al., 2020). Undoubtedly, the growing realization of low-cost hand-made devices is possible only thanks to the development of low-cost microcontrollers like Arduino, Beagleboard, or Raspberry (Harnett, 2011; Pearce, 2012), the advancement in additive manufacturing (Baden et al., 2015) and the rapid advances in electronic technologies that have led the availability of sensors and auxiliary components at affordable prices (Fisher & Gould, 2012; Mao et al., 2019).

In this sense, the agricultural engineering field was particularly fruitful and, over the years, very diversified low-cost self-made devices with different applications have been proposed. Just to recall some of them, Facchi et al. (2017) presented a device for the measurement of soil evaporation in aerobic rice fields, Masseroni et al. (2016) proposed an open-hardware tool for the continuous monitoring of soil water

potential in the root zone, Ravazzani (2017) developed a portable probe for the quantification of the soil moisture, while Chiaradia et al. (2015) realized a multisensory system for the continuous monitoring of water dynamic in rice fields.

One of the most important hydraulic parameters to control is water level, which can be useful for several applications, such as water flow monitoring and management, prediction of flood and drought and smart agriculture (Illes et al., 2013; Loizou & Koutroulis, 2016; Tscheikner-Gratl et al., 2019; Vijay Hari Ram et al., 2015). Considering the hydraulic engineering sector, there are a plethora of instrumentations devoted to this goal, i.e. staff gauges, electric-tape gauges, float-tape gauges, pressure transducers, or acoustic transducers (Herschy, 2009). However, these instruments generally are placed in a dedicated fixed installation, and therefore they are impractical to be transported in different in-situ locations, as it happens instead in the most common agricultural applications. In the last decade, different in-situ devices for water level measurements have been proposed, based on video surveillance (Noto et al., 2021; Schoener, 2018; Z. Zhang et al., 2019), low-cost sensors (Ezenne & Okoro, 2019; Hund et al., 2016; Loizou et al., 2015), low-cost GNSS antenna arrays (Purnell et al., 2021) and unmanned aerial vehicle (Gao et al., 2019; Ichikawa et al., 2019). Nevertheless, it is not so common to find low-cost devices that are also robust, easy to transport, install and disassemble and, at the same time, sufficiently accurate. With this purpose in mind, we present ArduHydro, a low-cost self-made open-access device for the monitoring of water levels that is a compact, robust, and very versatile instrument that can be installed in different ways on-site and easily removed to download the data.

This work is composed as follows: after this brief introduction, Section 2 describes in great detail how ArduHydro is composed and its functioning (Section 2.1), the open-channel flume facility used to assess the quality of the measurements (Section 2.2), and the agricultural field in which an example of field application is presented (Section 2.3). Section 3 is dedicated to showing and discussing the methodology for the data processing and then the output from the laboratory (Section 3.1) and in-field (Section 3.2) measurements. Finally, Section 4 summarizes the main outcomes.

2 Material And Methods

2.1 The ArduHydro device

The idea underpinning ArduHydro is to have a compact and versatile tool to monitor the water depth in different contexts. The sensor chosen to obtain the measurement is an ultrasonic range finder. To now, this type of sensor presents the best performance-to-price ratio on the market (Cherqui et al., 2020) and they are widely used in many applications with the most disparate purposes. In the following, all the information about the hardware, the software program, the specification of the sensors, and the cost of the components are described in detail.

2.1.1 Microcontroller board

The microcontroller board is based on the open-source *Arduino Nano* system and consists of a microcontroller (MCU) equipped with a bootloader for programming, a built-in support for serial communication (FTDI chip), and other complementary components such as a power supply regulator, Mini-USB connector, digital and analog pins for interfacing with external devices (e.g. sensors). The board can be powered with an unregulated power supply via the “Vin” pin (7 – 12V), with a regulated 5V power supply via the “5V” pin, or using the mini-USB connector (5V). The MCU is an ATmega328P microcontroller (Atmel Corporation, San Jose, Calif., USA) that features 14 digital ports and 6 analog ports, which can be used as inputs (e.g. for sensor reading) or outputs, with an operating voltage of 0 – 5V. The ATmega328P operates at a frequency of 16mHz and has 32 KB of flash memory, which serves as storage for the main operating program, as well as 1 KB EEPROM. The writing, compiling, and uploading of a program to the MCU can be easily carried out using an open-source integrated development environment (IDE)[1].

2.1.2 Power supply

The board is powered using a 9V Li-ion battery with a total capacity of 650mAh and is used in turn to power all external modules and sensors through the “3.3V” and “5V” pins as shown in Fig. 1. The battery has a Micro-USB socket for quick and convenient recharging via USB cable. When the device is not in use, the power supply can be interrupted using a simple SPST switch. The average power consumption of the device is around 25 mA, which means the theoretical battery life is 26 hours of continuous usage.

2.1.3 Sensors

As shown in Fig. 1, the microcontroller board is connected to two sensors: an ultrasonic range finder and a digital thermometer.

The ultrasonic range finder is an HY-SRF05 model, with a supply voltage of 4.5 – 5.5V and a digital pin interface. The sensor, working as both an ultrasound transmitter and receiver, can be used to measure distance in a range between 0.02 and 4.5 m with resolution up to 0.2 cm, a maximum measurement is 40 Hz, and a detection angle of 15°.

The digital thermometer is a DS18B20 model, with a 3-5.5V supply voltage, 1 wire bus interface, measuring range from − 55°C to + 125°C, ± 0.5°C accuracy, and resolution up to 0.0625°C. The sensor is contained in a waterproof stainless steel enclosure.

2.1.4 Datalogging

To allow long-term storage of measured data, the device is equipped with a MicroSD card reader module. The module can be used to transfer data to an external memory cartridge (MicroSD) via an SPI interface. The voltage needed to power the MicroSD reader is between 4.5 and 5.5 V. Due to the nature of the collected data, consisting of small-size text files, relatively low-profile storage cards are sufficient. For our purposes, a 256 Mb card was used for data logging.

Due to the lack of an internal clock on the microcontroller board, a DS3231 Real-Time-Clock (RTC) module was added to the device for data logging. This module features an integrated temperature-compensated crystal oscillator (TCXO) for higher accuracy. For timekeeping, the RTC needs a constant power supply with a voltage of 3.3 V, which is provided by the microcontroller board when the device is switched on, and by a CR2032 backup battery when the device is switched off.

2.1.5 Enclosure

All electronic components are fitted in a 100X100X50 mm plastic enclosure with IP56 protection, which protects against impacts and weather. The two sensors are positioned in the lower part of the enclosure, with the ultrasound transmitter/receiver of the HY-SRF05 and the waterproof probe section of the DS18B20 being the only parts exposed (Fig. 2a). The main switch is mounted on the upper part of the enclosure (with a silicone cover for waterproofing), alongside a small bubble level which facilitates the correct positioning of the device (Fig. 2b). This configuration allows ArduHydro to operate in unfavorable weather conditions with minimal risks of damage to the electronic components.

Table 1
List of ArduHydro components (updated to October 2022).

Name	Function	Supplier	Cost (€)	Batch cost (€)
Nano V3.0 CH340	Microcontroller	Az-Delivery	9.99	6.99
HY-SRF05	Ultrasonic sensor	HitLetGo	7.99	4.33
DS18B20	Temperature sensor	Az-Delivery	5.99	3.39
RTC DS3231	RTC Module	Az-Delivery	7.99	4.59
MicroSD Card Adapter	MicroSD reader	Az-Delivery	3.99	1.89
9V Li-ion rechargeable battery	Battery	ENEGON	10.50	9.49
Other components	Various	Local hardware stores	5.90	5.90
Total			**52.35**	**36.58**

2.1.6 Costs

The cost of each component used for building an ArduHydro device is shown in Table 1. The price shown under the Cost column refers to the purchase of a single component. For this study, ten ArduHydros were built, reducing the cost of individual components through batch purchases. The batch cost for each component is shown in the Batch cost column.

2.1.7 Operating principle

When measuring water levels, ArduHydro is mounted 2–450 cm above the water with the lower part directly facing the water surface and parallel to it. The distance between the sensor and the ground is then manually measured employing a graduate rod (precision ± 1 mm) and noted down. Once the device is switched on, the microcontroller board controls the operation of each component according to a program, called “sketch”, which was uploaded to the MCU via Arduino IDE and USB serial interface, as explained in Section 2.1.1. The sketch consists of two parts: “setup” and “loop”. The setup mainly consists of the initialization of libraries (packages with built-in functions) and the declaration of variables and is only executed once after the device is powered (this usually takes a few seconds), whereas the loop contains the main operating functions of the device, and is repeatedly executed in its entire length until the device is powered off. During the initial setup, a .txt file is created on the MicroSD to use for permanent storage of acquired data. The first operation carried out by ArduHydro in the loop segment of the sketch is temperature measurement via the DS18B20 sensor. This parameter is used to calculate the speed of sound in air as shown in Eq. (1) (Wong & Embleton, 1985):

$$c = \sqrt{\frac{\gamma R T}{M}}$$

1

where c (m/s) is the speed of sound, γ is the specific heat ratio, R (j/(mol*K)) is the universal gas constant, T (K) is the absolute temperature, and M (kg/mol) is the molar mass of air. Since $\gamma = 1.4$, $R = 8.3145$ J/K mol, and $M = 0.028966$ kg/mol (Hilsenrath et al., 1955), Eq. (1) becomes:

$$c = 20.05\sqrt{T}$$

2

Subsequently, the MCU sends a 10 µs HIGH signal at the Trigger pin (Trig) of the HY-SRF05 sensor. This prompts the ultrasonic transducer to emit a 40 kHz ultrasonic wave. If the wave encounters the water surface (or any other solid obstacle), it is reflected toward the sensor’s receiver. Once the return wave is detected, the sensor returns the value of the time elapsed since the emission of the wave (time of flight), which is then used to calculate the distance between the sensor and the water as follows:

$$d = \frac{ct}{2}$$

3

where d (m) is the distance and t (s) is the time of flight. Lastly, a string variable consisting of the date and time, t and d (separated by commas) is created and printed on a new line of the .txt file on the MicroSD. The loop segment is then repeated until the device is powered off, with each cycle lasting 0.2 seconds. This means that ArduHydro has a measuring frequency of 5 Hz. Once data is retrieved from the

MicroSD card, the values of distance from the water surface can be used to calculate the water level as shown in Eq. (4):

$$h = L - d$$

4

where h (m) is the water depth and L (m) is the distance between the sensor and the ground. In case the device is permanently mounted at a fixed position, this last procedure can be integrated within the sketch, in order to directly record the water depth values in the datalog file. However, this was not the case in the context of our study.

2.2 Laboratory experimental set-up

To quantify the performance of ArduHydro (AH) devices in measuring water levels, we have conducted a series of experiments aimed to test the devices in different hydraulic conditions. The experiments were carried out in a non-tilting, recirculating, open-channel flume at the Hydraulics Laboratory of the University of Pavia (Fig. 3). Furthermore, Fig. 3 reports the origin of the axes coordinate system used in the present study (i.e. the longitudinal x and vertical y directions). The main part of the facility is composed of a rectangular channel, which is 8.50 m long, 0.49 m wide, and 0.75 m deep. The flume has transparent Polymethyl methacrylate (PMMA) sidewalls and a metallic bed. The water levels h inside the flume are regulated through a vertical sluice gate placed at the end of the facility. The incoming flow rate Q, controlled by the presence of a gate valve in the delivery pipe, is measured upstream of the main part of the flume by means of a triangular-notch Thomson weir using (Shen, 1981):

$$Q = C\frac{8}{15}\sqrt{2g}\tan\left(\frac{\theta}{2}\right)h_w^{5/2} \qquad (5)$$

where C is the non-dimensional coefficient of discharge, g is the acceleration due to gravity, θ is the angle between the two sides of the notch (expressed in degrees) and h_w upstream piezometric head measured with respect to the vertex of the notch. For this specific weir,C and θ are equal to 0.72 and 36°, respectively. The piezometric head h_w is estimated with the aid of a manual piezometer equipped with a sharp point gauge connected to a vernier caliper (accuracy of 0.05 mm) placed in proximity to the triangular-notch Thomson weir. The distance between the channel bottom and the vertex of the notch is 0.152 m. A dissipation basin realized with a series of holed concrete blocks is placed downstream of the falling water coming from the weir to reduce the energy and turbulence of the flow approaching the inlet of the flume (Fig. 3). During some tests, a floating breakwater device realized in polystyrene was used to further reduce the free-water surface oscillations.

The position of the three AH devices involved in the experiments is shown in Fig. 3 together with the displacement of the four ultrasonic (US) distance sensors (PIL Sensoren GmbH, model: P43-F4V-2D-1C0-220E) used as a benchmark. Indeed ultrasonic distance sensors are widely used in laboratory applications concerning flows with a free surface and represent the standard in many situations (e.g.

Marino et al., 2018; Peruzzi et al., 2021; Zhang et al., 2018). The used USs (sampling frequency of 400 Hz) have a nominal accuracy of ± 1 mm that remains constant if the US works within its optimal sensing distance (i.e. between 8 and 160 cm away from the sensor). The ultrasonic signal emitted by the US propagates with a divergence angle equal to 8°. Another manual piezometer was placed close to the third US (Fig. 3) and used to have a further comparison.

In Section 3.1, the comparison between the AH sensor and the US sensor is made considering those in position 2 and in position 3 (Fig. 3), where a distance of 20 cm in the x direction between them was set. This distance is relatively low, hence possible differences between the water levels measured by the HA sensor (h_{AH}) and by the US sensor (h_{US}) due to hydraulic losses of the flow fall within the instrumental uncertainties. Furthermore, this distance ensures that the ultrasonic beams of the two sensors do not overlap.

2.2.1 Experimental procedure and hydraulic conditions

Table 2

Summary of experiments and associated hydraulic conditions. Q is the flow rate; h_p is the water depth measured by the downstream manual piezometer after the setting of the steady-state conditions; $U_b = Q/Wh_p$ is the bulk velocity estimated after the setting of the steady-state conditions, where W is the channel width, and $Fr = U_b/\sqrt{gh_p}$ is the Froude number, where g is the gravitational acceleration.

Run	Q [l/s]	h_p [cm]	U_b [cm/s]	Fr [-]	Duration	Floating Device
Exp 1	23.82	6.9	26.1	0.32	24 min 26 sec	No
Exp 2	36.76	15.2	27.7	0.23	14 min 03 sec	No
Exp 3	40.70	18.6	27.3	0.20	13 min 05 sec	No
Exp 4	23.65	6.8	26.0	0.32	23 min 10 sec	Yes
Exp 5	37.31	16.3	27.1	0.21	12 min 20 sec	Yes
Exp 6	41.06	19.5	26.8	0.19	10 min 58 sec	Yes

The water depths were measured during the entire duration of the six experiments listed in Table 2 by both the three AH and the four US sensors placed along the flume (Fig. 3). All the sensors were turned on simultaneously and, after that, the gate valve was opened in order to reach the desired flow rate. In this

way, the water stages were recorded in rather different moments, i.e., from the passage of the first wavefront to the establishment of the steady-state condition within the channel. The onset of the steady-state condition occurred when the water levels remain constant (within a range of ± 1.5 mm) at the downstream piezometer section. During the steady-state condition, the water depth at the downstream manual piezometer h_p and the bulk velocity U_b were estimated to characterize each experiment.

Exp 4 to 6 were conducted with the aid of the floating breakwater device in order to reduce the oscillation of the free surface.

2.3 Field experimental set-up

In addition to the laboratory test, an experiment in an outdoor environment was carried out evaluating the performance of the ArduHydro device for the detection of the waterfront advance (wavefront) during a surface irrigation. In particular an agricultural field located in the province of Mantua (Italy), whose details can be found in Masseroni et al. (2021; 2022), was considered as cases study (Fig. 4). The field is about 1.5 ha in size, divided into 4 borders of 30 m width and approximately 100 m length. Slope is about 0.61%. Closed-end border irrigation is the method for watering each border. Specifically, borders are irrigated by diverting a stream of water from the channel to the upper end of the border (point P1-4 in Fig. 4). The water flows down the slope and when the desired amount of water has been delivered to the border, the stream is turned off.

Ten AH sensors were installed along the longitudinal direction of the border (starting from the inlet point of irrigation flow rate) for detecting spatio-temporal wavefront evolution. The distance from the inlet of each sensor and its elevation from the ground are reported in Table 3. The elevation, useful for achieving water depth through Eq. (4), was measured manually using a graduated rod (precision ± 1 mm), while a thin wooden board was inserted at the base of each post to have a uniform level of the ground under the sensor.

The selected irrigation event was carried out on July 20, 2021. It was characterized by a flowrate of 367.4 l/s supplied for the examined border (i.e. border 2) for a duration of 48 minutes.

Table 3
Arrangement information of the AH sensors reported in Fig. 4 for the irrigation event of July 20, 2021.

# of AH sensor	Distance from the previous AH sensor	Progressive distance from the inlet	Elevation from the ground
1	0	10	30.8
2	5	15	31.9
3	5	20	32.8
4	5	30	36.2
5	10	40	33.4
6	10	50	28.0
7	10	60	33.5
8	10	70	29.0
9	15	85	31.5
10	15	100	30.5

[1] freely downloadable at http://www.arduino.cc

3 Results And Discussion

3.1 Results from the laboratory campaign

Before comparing the measurements performed by AH with those carried out by US device, two data filtering methods were employed to eliminate artefacts and outliers from AH collected raw data. At first, a simple data range filter was used, removing all negative values and all measurements exceeding the manually measured distance from the open-channel flume's bed. The second procedure was used to remove all errors attributable to delayed signals caused by uneven reflection on the water surface, which resulted in longer measured distances and consequently lower water levels. This involved calculating the moving maximum with a range of 10 measurements (2 seconds) and removing all data being more than 10% lower than this value. An example of the results achieved by the application of the two filtering methods is shown in Fig. 5, where AH raw and processed data are compared with US measurements.

Figure 6 shows the evolution of the water levels during each laboratory experiment. It can be noted a good agreement between the water levels measured by the US and AH sensors. As expected, Exps 1–3 (Fig. 6a-c) show a higher fluctuation of the free surface concerning the other tests (Exps 4–6, Fig. 6d-e), where a floating breakwater device was inserted. In this way, it was possible to assess the performance of the AH sensors in different free surface flow conditions. In general, the US seems to be more accurate to catch the small fluctuations of the free surface and this can be explained by the fact that the instrument measures by averaging the free surface fluctuations in a smaller area with respect to the AH sensors.

Depending on the experimental conditions (Table 2), the water level datum is inferred over an area of 76.30–106.26 cm^2 with the USs against an area of 215.55–311.35 cm^2 by using the AHs.

Furthermore, it can be seen from Fig. 6 how an unsteady phenomenon starts to occur in the first minutes of each Exp (hereinafter referred to as 'transient flow'). Specifically, a hydraulic jump takes place that moves from the downstream end of the flume to the upstream end due to the obstruction caused by the presence of the sluice gate. In the following, although this transient flow is well described also by the AH sensors, we omit to quantitatively compare the US and AH measurements during the passage of this unsteady flow since the distance of 20 cm in the longitudinal direction between the US and AH sensors (see the discussion in Section 2.2) become relevant and hence it can induce misinterpretation of the data.

To better understand the performance of the AH sensors, Fig. 7 reports the measured water levels by the two types of sensors in a scatter plot diagram. The data used for the comparison are only those that were recorded exactly at the same time by both sensors in positions 2 and 3 in the flume (Fig. 3). From these scatter plots, we can throw down the following indications: the AHs sensors are more accurate (i) as long as the free surface becomes smoothers and (ii) as long as the distance between the free surface and the AH sensor decreases. For what concerns the first statement, it is evident a less scatter in the data by comparing, for instance, Fig. 7a with Fig. 7d. Considering the second statement, the AHs performance strongly increases from Exp 1 to Exp 3 (Fig. 7a and Fig. 7c), where the distance between the sensor and the water is reduced by about 15 cm. Thus, although the sensor mounted in the AH works with a wide range of distances (2–450 cm as reported by the manufacturer, see Section 2.1.3), to properly measure water levels, the optimal distance seems to be around 55 cm from the free surface.

Table 4

Pearson correlation coefficient r, coefficient of determination R^2, and root-mean-square error $RMSE$ for the two investigated positions.

	Comparison 2 AH – 2 US			Comparison 3 AH – 3 US		
	r [-]	R^2 [-]	$RMSE$ [cm]	r [-]	R^2 [-]	$RMSE$ [cm]
Exp 1	0.835	0.669	0.540	0.820	0.504	0.532
Exp 2	0.974	0.930	0.874	0.962	0.915	0.959
Exp 3	0.994	0.987	0.643	0.985	0.969	0.999
Exp 4	0.990	0.978	0.294	0.989	0.977	0.289
Exp 5	0.994	0.989	0.451	0.993	0.987	0.495
Exp 6	0.997	0.993	0.564	0.994	0.988	0.752

Table 4 shows the results of some quantitative statistical indicators used to further characterize the AHs performance, i.e. the Pearson correlation coefficient r, the coefficient of determination R^2 and the root-mean-square error $RMSE$ that are defined as (Dawson et al., 2007):

$$r = \frac{1}{N-1}\sum_{i=1}^{N}\left(\frac{h_{AH_i}-\mu_{h_{AH}}}{\sigma_{h_{AH}}}\right)\left(\frac{h_{US_i}-\mu_{h_{US}}}{\sigma_{h_{US}}}\right)$$

(6)

$$R^2 = 1 - \frac{\sum_{i=1}^{N}\left(h_{US_i}-h_{AH_i}\right)^2}{\sum_{i=1}^{N}\left(h_{US_i}-\mu_{h_{US}}\right)^2}$$

(7)

$$RMSE = \sqrt{\frac{1}{N}\sum_{i=1}^{N}\left(h_{US_i}-h_{AH_i}\right)^2}$$

(8)

where $\mu_{h_{AH}}$ and $\sigma_{h_{AH}}$ are the mean and standard deviation of h_{AH}, respectively, and $\mu_{h_{US}}$ and $\sigma_{h_{US}}$ are the mean and standard deviation of h_{US}, while N is the size of the dataset. Eqs. (6)–(8) were computed considering the dataset shown in Fig. 7 without the transient flow (grey dots).

From Table 4 we can see that the comparison between AH and US sensors in position 2 and position 3 gives pretty much the same outcome, showing that the results are independent of the spatial position along the flume. As already noted in Fig. 7, Exp 1 shows the worst scenario, where the free surface has the biggest fluctuations and the greatest distance from the sensor. In this situation, R^2 is rather low, giving a mean value of 0.6 and a root-mean-square percentage error, i.e. $100 \bullet \left(RMSE/\mu_{h_{US}}\right)$, equal to 7.7%. On the opposite side, all the other Exps show an $R^2 > 0.91$ with a root-mean-square percentage error in the range 2.9–6%, depending on the test.

3.2 Results from the field campaign

In this section, we present a potential application of the ArduHydro sensors in the agricultural water management field. As pointed out by Masseroni et al. (2017), surface irrigation practices, still largely adopted in the world for watering row crops, cannot be completely replaced by modern pressure systems since they give important and positive externalities in terms of ecosystem services to the surrounding environment and landscape. However, increasing the efficiency of surface irrigations (such as border irrigation), is desirable and needed in light of the effect of climate change is having on the availability of water resources for irrigation (Chen et al., 2013; Masseroni et al., 2022).

In this scenario, AH sensors can be involved as an advantageous tool to measure the water levels within a crop field and hence to quantitatively characterize the irrigation, both from a spatial and temporal point of view. That information can then be used to calibrate and validate models useful to guide the decisionmaker to establish scientific-based guidelines for the farmers (Costabile et al., 2022).

As an example, here we report the evolution of the irrigation wavefront (Fig. 8) measured during a border irrigation event on July 20, 2021. As it can be noted, the AH sensors are highly reactive in recording the passage of the wave, and, also from this simple measurement, important considerations can be highlighted. In general, the evolution of water depth onto the field registered by each sensor is consistent with the expectation. More in detail, the water depth rapidly increases when the wavefront reaches the sensor; it remains approximately constant during the wetting phase and then decreases because of the combination of wavefront lateral dispersion and infiltration. On average, a decreasing trend of the maximum water depth is registered from the inlet point to the border ends. However, some singularities, typical of a water propagation onto a tilted rough surface, are evidenced. For instance, the last two sensors (9 AH and 10 AH) measured higher water levels with respect to the one right before (8 AH). The possible explanation is that there is a reduction in the field slope and/or an increasing of surface roughness that leads to a reduction of wavefront velocity and to an increasing of water depth. The same behavior is evidenced in the 7 AH sensor in respect to the 6 AH sensor as a result of non-uniformity of surface roughness characteristics onto the field.

Data obtained from this experimental campaign by using of AH devices as water level detector could be employed to better understand border irrigation dynamics and in particular to describe both waterfront advance and recession, calculate the intake opportunity time, estimate uniformity of water distribution onto the field or calibrate hydrodynamical models (Salahou et al., 2018).

4 Conclusions

We have presented a novel handmade low-cost sensor called ArduHydro to measure and monitor the water level in almost all situations where it is not possible to install fixed stations. The strengths of ArduHydro are: (i) the low-cost (around 50 euros for a single sensor or around 35 euros each for batch of 10 sensors); (ii) based on the open-source Arduino technology, hence it is fully customizable to the user's needs in terms of sampling frequency rate and processing of the data; (iii) it is robust, compact, and easy to carry, therefore, suitable to work in extreme conditions; (iv) very precise when the distance from the free surface is around 50 cm or less, having an $R^2 > 0.91$ and a root-mean-square percentage error lower than 6% if we compare the output data with the state-of-the-art laboratory ultrasonic sensor. This sensor can be used in many applications and here we have presented a possible one, i.e., the monitoring of water levels during border irrigation. Thanks to the ArduHydro sensor, it was possible to measure the advancement of the irrigation wavefront directly inside the field and hence collect important data to aid the modelling surface irrigation dynamics.

Declarations

Acknowledgements

The Authors gratefully acknowledge Prof. Eng. S. Sibilla, Prof. Eng. P. Ghirardi, Prof. Eng. G. Petaccia, Dr. Eng. A. Fenocchi and Dr. Eng E. Persi (University of Pavia) for allowing and supporting us to perform the laboratory experiments in the open-channel flow facility presents at their Hydraulics Laboratory. The landowners Remelli and Dalzini are thanked for allowing their land to be exploited for scientific research purposes. Finally, the Authors warmly thank the technicians of the Consorzio di Bonifica Garda Chiese for their important support provided during the field measurements.

Authors’ contributions

Andrea Galli: Conceptualization, Validation, Formal analysis, Data Curation, Visualization, Investigation, Writing - Original Draft, Writing - Review & Editing.

Cosimo Peruzzi: Conceptualization, Validation, Formal analysis, Data Curation, Visualization, Investigation, Supervision, Writing - Original Draft, Writing - Review & Editing.

Fabiola Gangi: Formal analysis, Data Curation, Visualization, Investigation, Writing - Review & Editing.

Daniele Masseroni: Conceptualization, Methodology, Supervision, Project administration, Funding acquisition, Writing - Original Draft, Writing - Review & Editing.

Funding

This work was developed in the context of the MONAIISa project (mathematical MOdels and NAture-based solutions for Improving combined Sewer overflows management and reuse) funded by

Fondazione Cariplo, Italy (grant number 2019-2084) and the IrriGate project (Toward smart and flexible irrigation management in gravity-fed irrigation contexts) funded by Regione Lombardia, Italy (grant number 2019-01319885).

Competing interests

The authors declare that they have no known competing financial interests or personal relationships that could have appeared to influence the work herein reported.

Availability of data and materials

All the data used in this study are available, upon request, by contacting the corresponding author.

References

1. Baden, T., Chagas, A. M., Gage, G., Marzullo, T., Prieto-Godino, L. L., & Euler, T. (2015). Open Labware: 3-D Printing Your Own Lab Equipment. *PLoS Biology*, *13*(3), 1–12. https://doi.org/10.1371/journal.pbio.1002086
2. Chen, B., Ouyang, Z., Sun, Z., Wu, L., & Li, F. (2013). Evaluation on the potential of improving border irrigation performance through border dimensions optimization: A case study on the irrigation districts along the lower Yellow River. *Irrigation Science*, *31*(4), 715–728. https://doi.org/10.1007/s00271-012-0338-0
3. Cherqui, F., James, R., Poelsma, P., Burns, M. J., Szota, C., Fletcher, T., & Bertrand-Krajewski, J. L. (2020). A platform and protocol to standardise the test and selection low-cost sensors for water level monitoring. *H2Open Journal*, *3*(1), 437–456. https://doi.org/10.2166/h2oj.2020.050
4. Chiaradia, E. A., Facchi, A., Masseroni, D., Ferrari, D., Bischetti, G. B., Gharsallah, O., Cesari de Maria, S., Rienzner, M., Naldi, E., Romani, M., & Gandolfi, C. (2015). An integrated, multisensor system for the continuous monitoring of water dynamics in rice fields under different irrigation regimes. *Environmental Monitoring and Assessment*, *187*(9). https://doi.org/10.1007/s10661-015-4796-8
5. Costabile, P., Costanzo, C., Gangi, F., De Gaetani, C. I., Rossi, L., Gandolfi, C., & Masseroni, D. (2022). High-resolution 2D modelling for simulating and improving the management of border irrigation. *Under Review*.
6. Dawson, C. W., Abrahart, R. J., & See, L. M. (2007). HydroTest: A web-based toolbox of evaluation metrics for the standardised assessment of hydrological forecasts. *Environmental Modelling and Software*, *22*(7), 1034–1052. https://doi.org/10.1016/j.envsoft.2006.06.008
7. Ezenne, I. G., & Okoro, O. G. (2019). Development of a Low Cost Automatic Water Level Monitoring System. *Agricultural Engineering International: CIGR Journal*, *21*(3), 1–6.
8. Facchi, A., Masseroni, D., & Miniotti, E. F. (2017). Self-made microlysimeters to measure soil evaporation: a test on aerobic rice in northern Italy. *Paddy and Water Environment*, *15*(3), 669–680. https://doi.org/10.1007/s10333-016-0566-7

9. Fisher, D. K., Fletcher, R. S., & Anapalli, S. S. (2020). Evolving Open-Source Technologies Offer Options for Remote Sensing and Monitoring in Agriculture. *Advances in Internet of Things*, *10*(01), 1–10. https://doi.org/10.4236/ait.2020.101001
10. Fisher, D. K., & Gould, P. J. (2012). Open-Source Hardware Is a Low-Cost Alternative for Scientific Instrumentation and Research. *Modern Instrumentation*, *01*(02), 8–20. https://doi.org/10.4236/mi.2012.12002
11. Gao, A., Wu, S., Wang, F., Wu, X., Xu, P., Yu, L., & Zhu, S. (2019). A newly developed unmanned aerial vehicle (UAV) imagery based technology for field measurement of water level. *Water (Switzerland)*, *11*(1). https://doi.org/10.3390/w11010124
12. Harnett, C. (2011). Open source hardware for instrumentation and measurement. *IEEE Instrumentation and Measurement Magazine*, *14*(3), 34–38. https://doi.org/10.1109/MIM.2011.5773535
13. Herschy, R. W. (2009). *Streamflow Measurement* (3rd ed.). Taylor & Francis.
14. Hilsenrath, J., Beckett, C. W., William, S. B., Fano, L., Hoge, H. J., Masi, J. F., Nuttall, R. L., Touloukian, Y. S., & Woolley, H. W. (1955). *Tables of Thermal Properties of Gases* (Circular 5). US Department of Commerce, National Bureau of Standards.
15. Hund, S. V., Johnson, M. S., & Keddie, T. (2016). Developing a Hydrologic Monitoring Network in Data-Scarce Regions Using Open-Source Arduino Dataloggers. *Agricultural & Environmental Letters*, *1*(1), 160011. https://doi.org/10.2134/ael2016.02.0011
16. Ichikawa, K., Ebinuma, T., Konda, M., & Yufu, K. (2019). Low-cost GNSS-R altimetry on a UAV for water-level measurements at arbitrary times and locations. *Sensors (Switzerland)*, *19*(5). https://doi.org/10.3390/s19050998
17. Illes, C., Popa, G. N., & Filip, I. (2013). Water level control system using PLC and wireless sensors. *ICCC 2013 - IEEE 9th International Conference on Computational Cybernetics, Proceedings*, 195–199. https://doi.org/10.1109/ICCCyb.2013.6617587
18. Loizou, K., & Koutroulis, E. (2016). Water level sensing: State of the art review and performance evaluation of a low-cost measurement system. *Measurement: Journal of the International Measurement Confederation*, *89*, 204–214. https://doi.org/10.1016/j.measurement.2016.04.019
19. Loizou, K., Koutroulis, E., Zalikas, D., & Liontas, G. (2015). A low-cost sensor based on time-domain reflectometry for water level monitoring in environmental applications. *2015 IEEE 15th International Conference on Environment and Electrical Engineering, EEEIC 2015 - Conference Proceedings*, 261–266. https://doi.org/10.1109/EEEIC.2015.7165549
20. Mao, F., Khamis, K., Krause, S., Clark, J., & Hannah, D. M. (2019). Low-Cost Environmental Sensor Networks: Recent Advances and Future Directions. *Frontiers in Earth Science*, *7*, 1–7. https://doi.org/10.3389/feart.2019.00221
21. Marino, M., Rabionet, I. C., Musumeci, R. E., & Foti, E. (2018). Reliability of Pressure Sensors To Measure Wave Height in the Shoaling Region. *Proceedings of the 36th International Conference on Coastal Engineering*, *36*, 10. https://doi.org/10.9753/icce.v36.papers.10

22. Masseroni, D., Castagna, A., & Gandolfi, C. (2021). Evaluating the performances of a flexible mechanism of water diversion: application on a northern Italy gravity-driven irrigation channel. *Irrigation Science*, *39*(3), 363–373. https://doi.org/10.1007/s00271-020-00718-8
23. Masseroni, D., Facchi, A., Depoli, E. V., Renga, F. M., & Gandolfi, C. (2016). Irrig-OH: An Open-Hardware Device for Soil Water Potential Monitoring and Irrigation Management. *Irrigation and Drainage*, *65*(5), 750–761. https://doi.org/10.1002/ird.1989
24. Masseroni, D., Gangi, F., Galli, A., Ceriani, R., De Gaetani, C., & Gandolfi, C. (2022). Behind the efficiency of border irrigation: Lesson learned in Northern Italy. *Agricultural Water Management*, *269*, 107717. https://doi.org/10.1016/j.agwat.2022.107717
25. Masseroni, D., Ricart, S., de Cartagena, F. R., Monserrat, J., Gonçalves, J. M., de Lima, I., Facchi, A., Sali, G., & Gandolfi, C. (2017). Prospects for improving gravity-fed surface irrigation systems in mediterranean european contexts. *Water (Switzerland)*, *9*(1). https://doi.org/10.3390/w9010020
26. Montanari, A., Young, G., Savenije, H. H. G., Hughes, D., Wagener, T., Ren, L. L., Koutsoyiannis, D., Cudennec, C., Toth, E., Grimaldi, S., Blöschl, G., Sivapalan, M., Beven, K., Gupta, H., Hipsey, M., Schaefli, B., Arheimer, B., Boegh, E., Schymanski, S. J., … Belyaev, V. (2013). "Panta Rhei-Everything Flows": Change in hydrology and society-The IAHS Scientific Decade 2013-2022. *Hydrological Sciences Journal*, *58*(6), 1256–1275. https://doi.org/10.1080/02626667.2013.809088
27. Noto, S., Tauro, F., Petroselli, A., Apollonio, C., Botter, G., & Grimaldi, S. (2021). Technical Note: Low cost stage-camera system for continuous water level monitoring in ephemeral streams. *Hydrology and Earth System Sciences Discussions*, 1–17. https://doi.org/10.5194/hess-2021-36
28. Pearce, J. M. (2012). Building research equipment with free, open-source hardware. *Science*, *337*(6100), 1303–1304. https://doi.org/10.1126/science.1228183
29. Persi, E., Petaccia, G., Fenocchi, A., Manenti, S., Ghilardi, P., & Sibilla, S. (2019). Hydrodynamic coefficients of yawed cylinders in open-channel flow. *Flow Measurement and Instrumentation*, *65*, 288–296. https://doi.org/10.1016/j.flowmeasinst.2019.01.006
30. Peruzzi, C., Vettori, D., Poggi, D., Blondeaux, P., Ridolfi, L., & Manes, C. (2021). On the influence of collinear surface waves on turbulence in smooth-bed open-channel flows. *Journal of Fluid Mechanics*, *924*, 1–37. https://doi.org/10.1017/jfm.2021.605
31. Purnell, D. J., Gomez, N., Minarik, W., Porter, D., & Langston, G. (2021). Precise water level measurements using low-cost GNSS antenna arrays. *Earth Surface Dynamics*, *9*(3), 673–685. https://doi.org/10.5194/esurf-9-673-2021
32. Ravazzani, G. (2017). Open hardware portable dual-probe heat-pulse sensor for measuring soil thermal properties and water content. *Computers and Electronics in Agriculture*, *133*, 9–14. https://doi.org/10.1016/j.compag.2016.12.012
33. Salahou, M. K., Jiao, X., & Lü, H. (2018). Border irrigation performance with distance-based cut-off. *Agricultural Water Management*, *201*, 27–37. https://doi.org/10.1016/j.agwat.2018.01.014
34. Schoener, G. (2018). Time-Lapse Photography: Low-Cost, Low-Tech Alternative for Monitoring Flow Depth. *Journal of Hydrologic Engineering*, *23*(2), 06017007. https://doi.org/10.1061/(asce)he.1943-

5584.0001616

35. Shen, J. (1981). Discharge Characteristics of Triangular-Notch Thin-Plate Weirs. In *US Geological Survey Water Supply Paper*. https://doi.org/10.3133/wsp1617B
36. Tauro, F., Selker, J., Van De Giesen, N., Abrate, T., Uijlenhoet, R., Porfiri, M., Manfreda, S., Caylor, K., Moramarco, T., Benveniste, J., Ciraolo, G., Estes, L., Domeneghetti, A., Perks, M. T., Corbari, C., Rabiei, E., Ravazzani, G., Bogena, H., Harfouche, A., … Grimaldia, S. (2018). Measurements and observations in the XXI century (MOXXI): Innovation and multi-disciplinarity to sense the hydrological cycle. *Hydrological Sciences Journal*, *63*(2), 169–196. https://doi.org/10.1080/02626667.2017.1420191
37. Toran, L. (2016). Water level loggers as a low-cost tool for monitoring of stormwater control measures. *Water (Switzerland)*, *8*(8). https://doi.org/10.3390/w8080346
38. Tscheikner-Gratl, F., Caradot, N., Cherqui, F., Leitão, J. P., Ahmadi, M., Langeveld, J. G., Le Gat, Y., Scholten, L., Roghani, B., Rodríguez, J. P., Lepot, M., Stegeman, B., Heinrichsen, A., Kropp, I., Kerres, K., Almeida, M. do C., Bach, P. M., Moy de Vitry, M., Sá Marques, A., … Clemens, F. (2019). Sewer asset management–state of the art and research needs. *Urban Water Journal*, *16*(9), 662–675. https://doi.org/10.1080/1573062X.2020.1713382
39. Vijay Hari Ram, V., Vishal, H., Dhanalakshmi, S., & Meenakshi Vidya, P. (2015). Regulation of water in agriculture field using Internet Of Things. *Proceedings - 2015 IEEE International Conference on Technological Innovations in ICT for Agriculture and Rural Development, TIAR 2015*, 112–115. https://doi.org/10.1109/TIAR.2015.7358541
40. Wickert, A. D., Sandell, C. T., Schulz, B., & Ng, G. H. C. (2019). Open-source Arduino-compatible data loggers designed for field research. *Hydrology and Earth System Sciences*, *23*(4), 2065–2076. https://doi.org/10.5194/hess-23-2065-2019
41. Wong, G. S. K., & Embleton, T. F. (1985). Variation of the speed of sound in air with humidity and temperature. *Journal of the Acoustical Society of America*, *77*(5), 1710–1712. https://doi.org/10.1121/1.391918
42. Zhang, G., Valero, D., Bung, D. B., & Chanson, H. (2018). On the estimation of free-surface turbulence using ultrasonic sensors. *Flow Measurement and Instrumentation*, *60*, 171–184. https://doi.org/10.1016/j.flowmeasinst.2018.02.009
43. Zhang, Z., Zhou, Y., Liu, H., & Gao, H. (2019). In-situ water level measurement using NIR-imaging video camera. *Flow Measurement and Instrumentation*, *67*, 95–106. https://doi.org/10.1016/j.flowmeasinst.2019.04.004

Figures

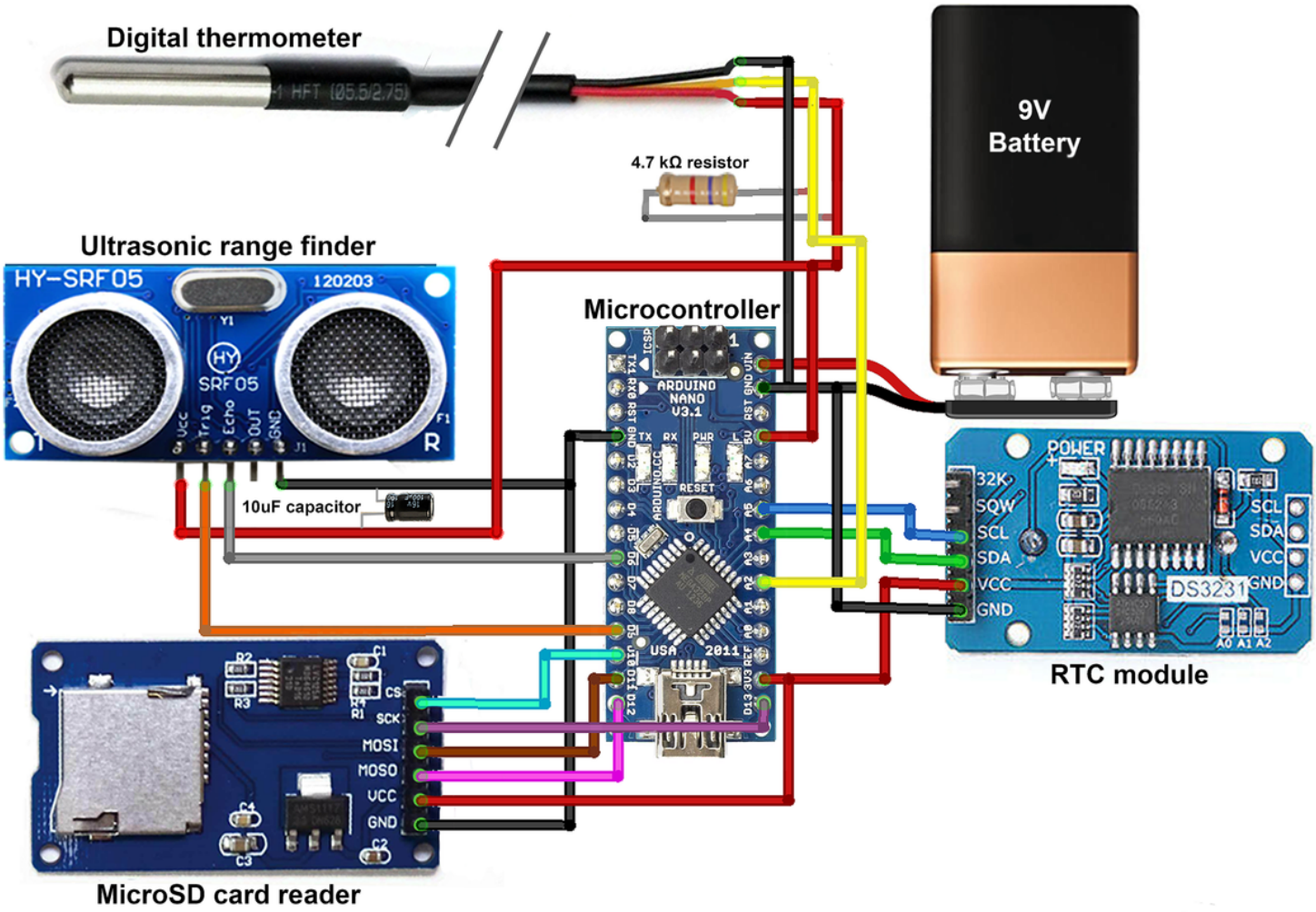

Figure 1

Wiring diagram of ArduHydro components

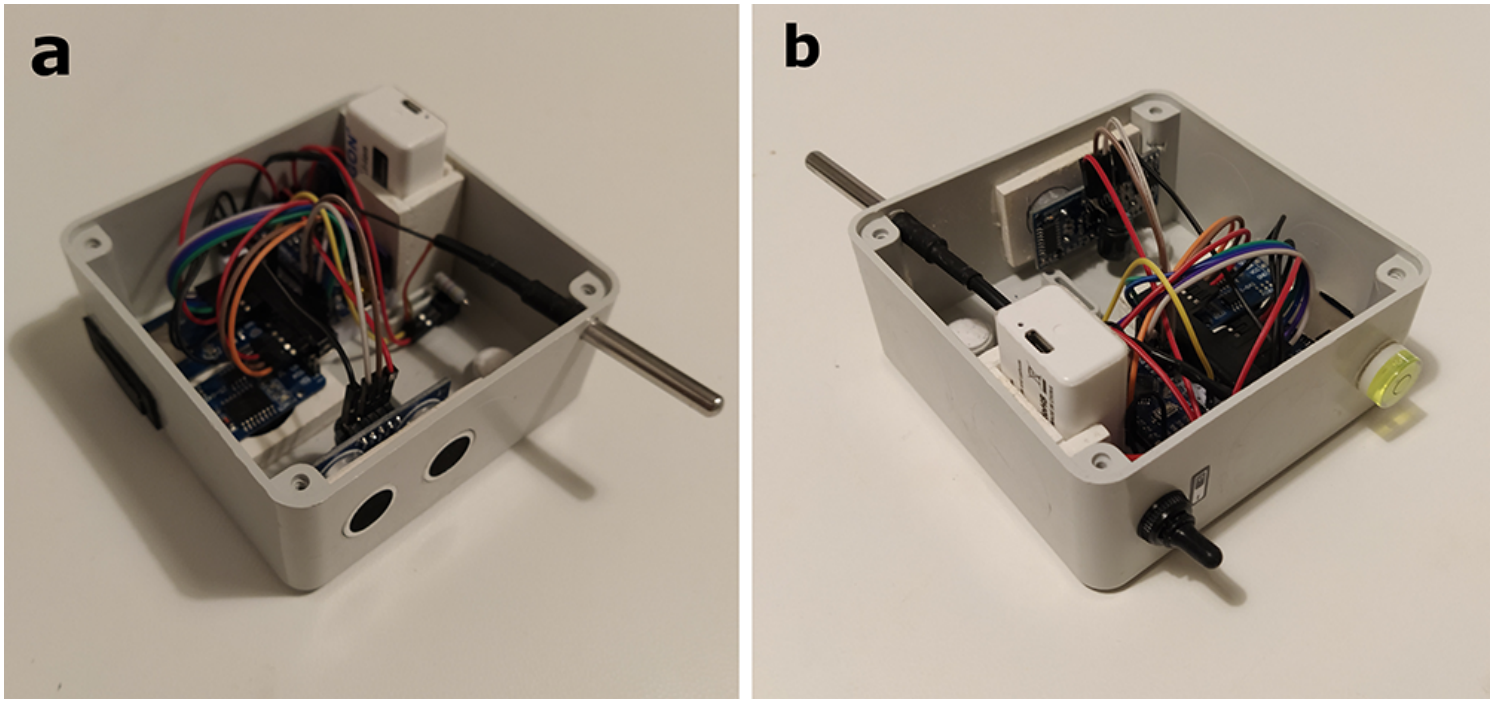

Figure 2

Inside view of ArduHydro; (a) lower part with sensors, (b) upper part with switch and bubble level.

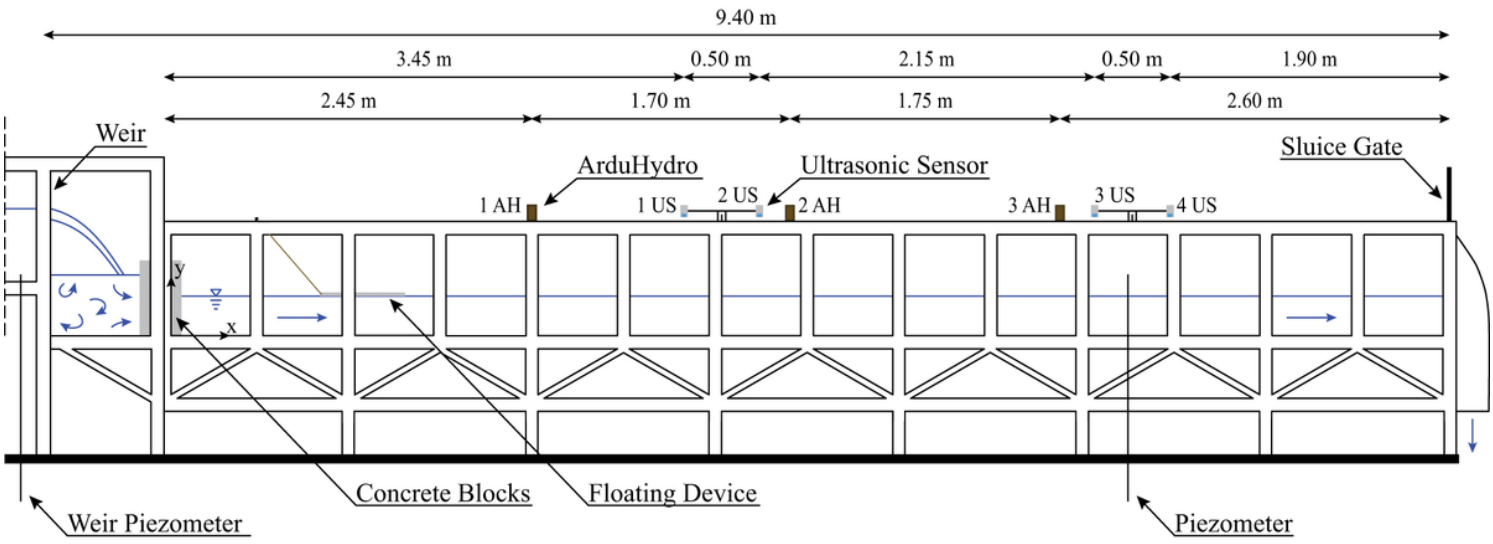

Figure 3

Sketch of the whole hydraulic circuit used in the experiments (adapted from Persi et al., 2019).

Figure 4

The agricultural field with the indication of the four sectors. The blue points indicate the water inlet whereas the yellow points represent the ArduHydro positions within the second sector.

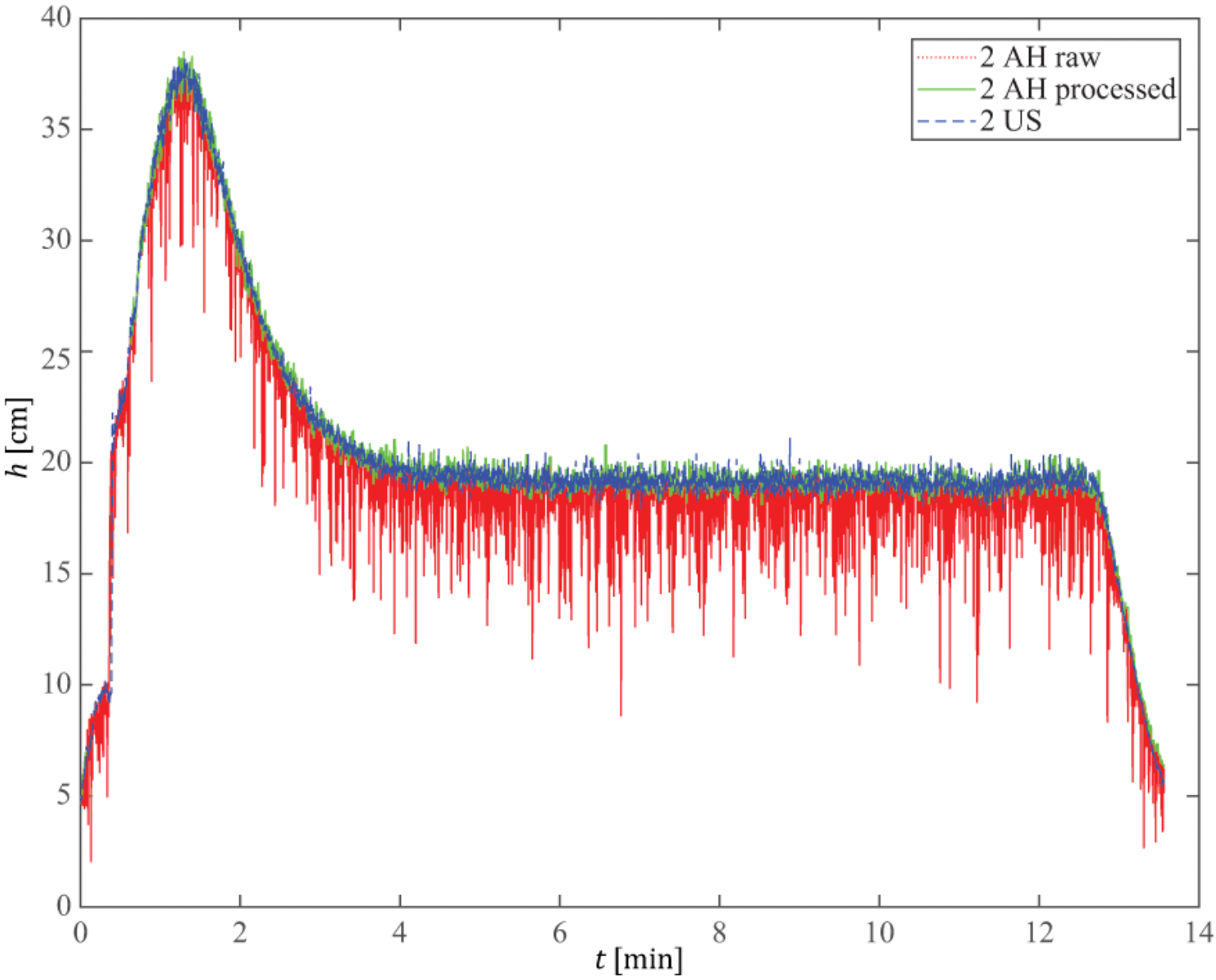

Figure 5

Data filtering results. Raw AH data are shown in red, while processed data and US data are shown in green and blue, respectively.

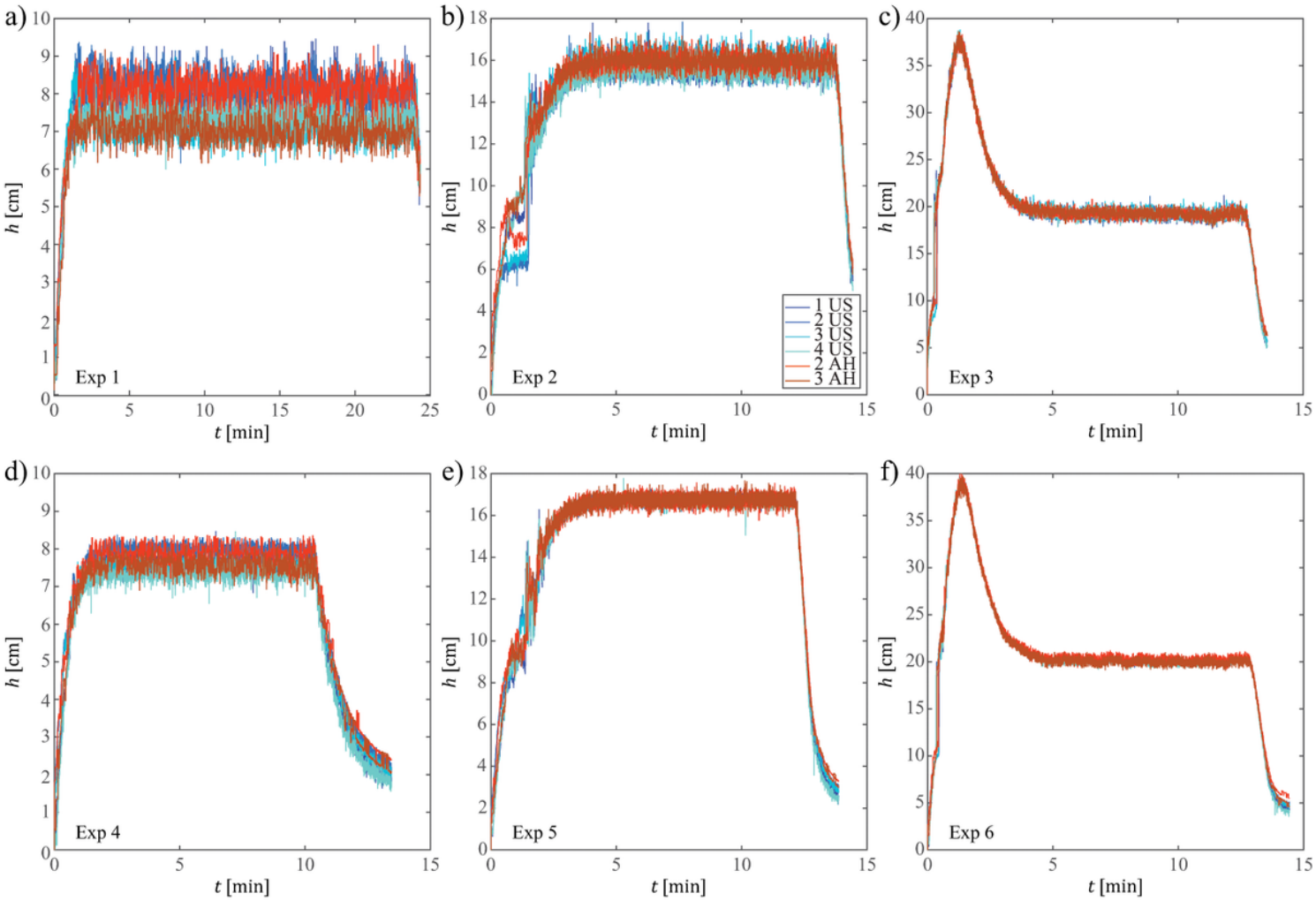

Figure 6

Free surface profiles for each experiment. The water levels measured by the 1 AH sensor are not reported for clarity purposes.

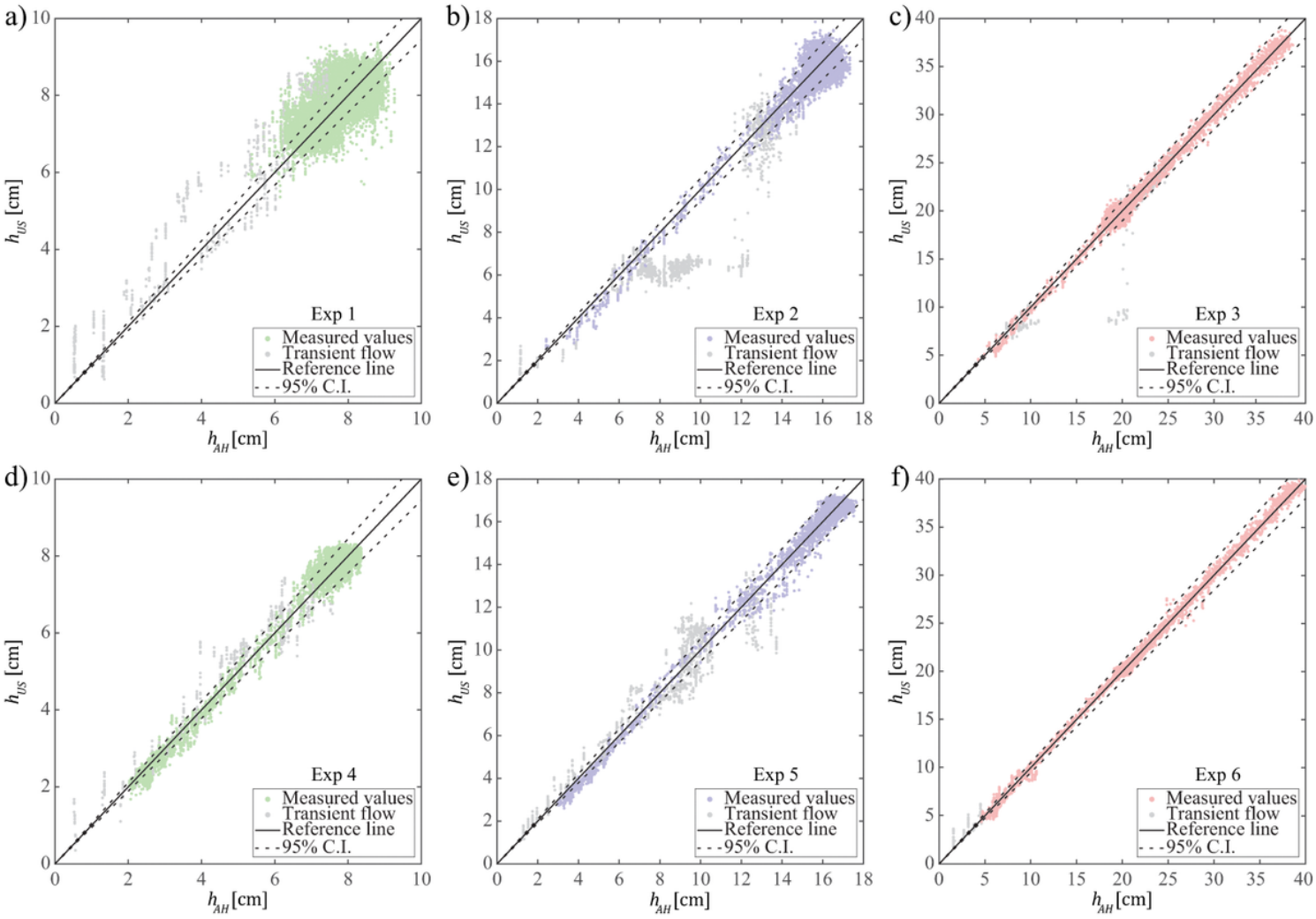

Figure 7

Scatter plot reporting the water levels measured by the AH sensors (h_{AH}) versus the water level measured by the US sensors (h_{US}) in the positions 2 and 3 (Figure 3). All the panels also display the data measured during the passage of the transient flow (grey dots).

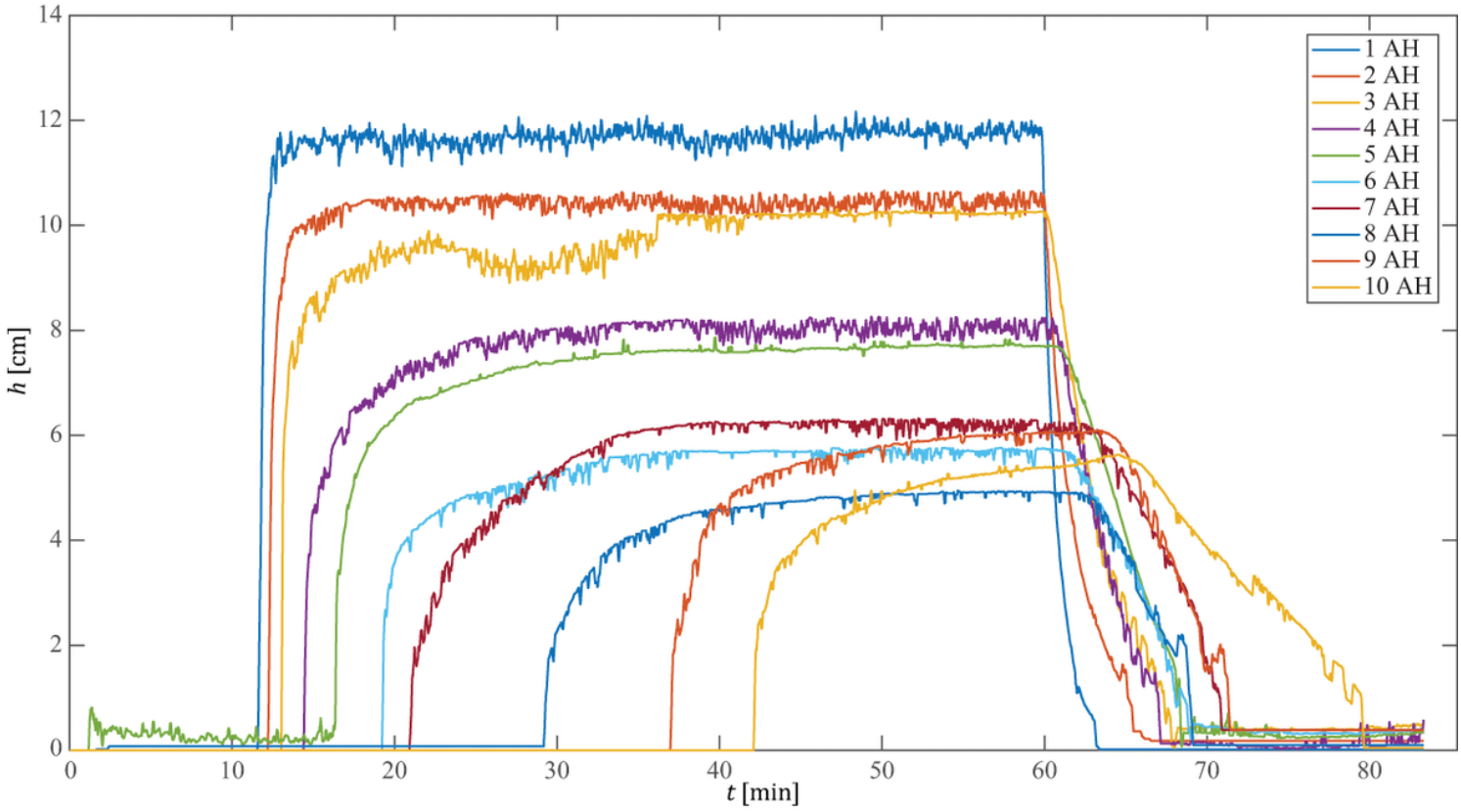

Figure 8

Evolution of the irrigational wavefront captured by the 10 AH sensors displaced along the sector.